Materials Science-Poland, Vol. 25, No. 4, 2007

Computer simulation and optimization of properties of porous low-*k* dielectrics*

A. ELSNER**, H. HERMANN

Institute for Solid State and Materials Research, IFW Dresden,
P.O. Box 270116, D-01171 Dresden, Germany

Due to progressive miniaturization one of the current challenges in microelectronics is to find materials with very low electric permittivity. The model of dense random packed spheres is applied to generate model systems of porous dielectric materials. Pores are represented by dense packed spheres. By optimizing the parameters, the porosity and therefore the theoretical electric permittivity was reduced significantly. Another task is optimization of mechanical properties. Mechanical stability is an important criterion for the processability in industrial fabrication of microlectronics components. The mechanical stability is mostly negatively correlated to porosity. Simulated open pore and closed pore systems with high porosity were analyzed in terms of mechanical properties. Other methods like an adapted random walk algorithm were used to characterize further important properties like particle permeability. In porous materials, the so-called "random voiding" may appear. This happens when pores are larger than the layer thickness. Simulation of porous structures can show limitations in pore size and spatial distribution where the requirements of industrial processability are no longer satisfied. Advantageous parameters for porosity in dielectric materials are advised.

Key words: *porous structure; low-k dielectrics; computer simulation; dense random sphere packings*

1. Introduction

Introducing porosity in dielectric materials is one of the most promising methods to decrease the static electric permittivity [1, 2]. Production of porous dielectric materials is a non-trivial task, because mechanical and processing properties often heavily change with degree of porosity. Computer simulation of porous materials may help to optimize porous structures relative to their mechanical and dielectric properties.

One of the most dreaded defects is the so-called voiding. There, pores appearing in the material are so large that they form a hole where gas or fluids can diffuse

---

*Presented at the 2nd Workshop "Hybrid Nanostructured Materials. Synthesis, Properties, Applications", Dresden, Germany, 8–9 November, 2006.

**Corresponding author, e-mail: A.Elsner@ifw-dresden.de

through [3]. To avoid this, the pore size distribution has to keep limiting conditions. Likewise, the penetrability by small particles plays a role. It is not desired that particles infiltrate the material because the dielectric properties may change or even short-circuits may appear.

Another simulation shall demonstrate the behaviour of porous dielectrics when investigated by positron annihilation lifetime spectroscopy (PALS) [4]. A non-lattice random walk method is applied to porous models as a first approach to simulate the way of positronium particles in the structure. Statistical analyzis of free ways and lifetimes of particles are compared with experimental results.

2. Generation of model systems

In a previous work [5], we studied random dense sphere packings generated by the force biased algorithm wherein the spheres constitute the pores and the space around these spheres is the base dielectric material, for example silicon dioxide. From experimental studies on porous silica gel, a power-law pore size distribution was estimated. The power-law size distribution with adjustable parameters was then used to analyze corresponding closed-pore systems (Eq. (1)). The computer simulation models were optimized with respect to the highest porosity. A local maximum of porosity could be obtained at an exponent of $a = -3.3$, $r_1 = 1.0$ and $r_2 = 5.0$.

$$f(r) = c\left(\frac{r}{r_0}\right)^a, \qquad r_1 \le r \le r_2 \tag{1}$$

Our model systems contain usually between 1000 and 10 000 spheres but larger systems of more than 10^6 pores can be easily calculated as well. The simulation volume is defined in 3D Cartesian coordinates. One corner of the simulation volume is placed at the origin, hence the whole volume is defined in positive coordinates. The boundary conditions are periodical in all three space dimensions. The sides of the simulation box are of arbitrary length; here we used a cubic box of 20 unit lengths in every direction.

Based on the fact that pore diameter distribution depends on the production process, various pore size distributions were analyzed. Here we study power-law and log –normal pore size distributions. These pore size distributions were applied in a wide parameter range and recommendations are given for optimum parameterization.

3. Structure optimization

As described in [1], we optimized power-law distributed pore systems in terms of maximum porosity. The packing fraction or porosity for this closed pore model was $P \approx 0.71$. Now we present another optimized system with log–normal diameter distri-

bution. We used heuristic methods and numerical methods like the Nelder–Mead simplex method [6] to optimize the packed sphere systems. Every simulation series included 1000 randomly distributed spheres. The pore diameters are log–normal distributed according to the probability density function:

$$f(x;\mu,\sigma) = \frac{1}{x\sigma\sqrt{2\pi}} \exp\left[-(\ln x - \mu)^2 / \left(2\sigma^2\right)\right] \tag{2}$$

Mean pore size was fixed at $\mu = 1.0$, the standard deviation was varied in steps of 0.1 in the range of 0.1 to 1.2. The task was to find the optimum value of standard deviation for this constellation. We found that for a standard deviation of $\sigma = 0.9$, the highest packing fractions around $P \approx 0.73$ were generated (Fig. 1), independently of diameter scaling.

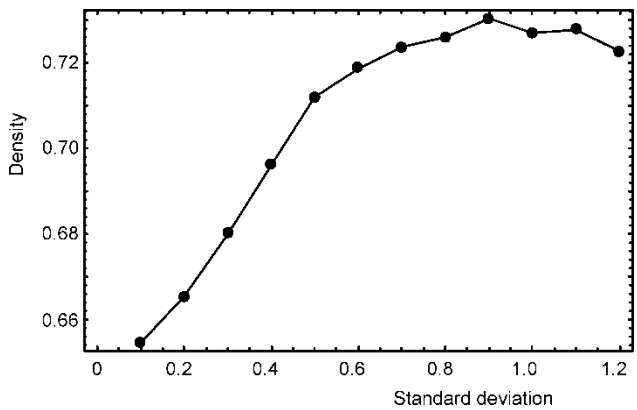

Fig. 1. Packing fraction vs. standard deviation for a log–normal distributed system

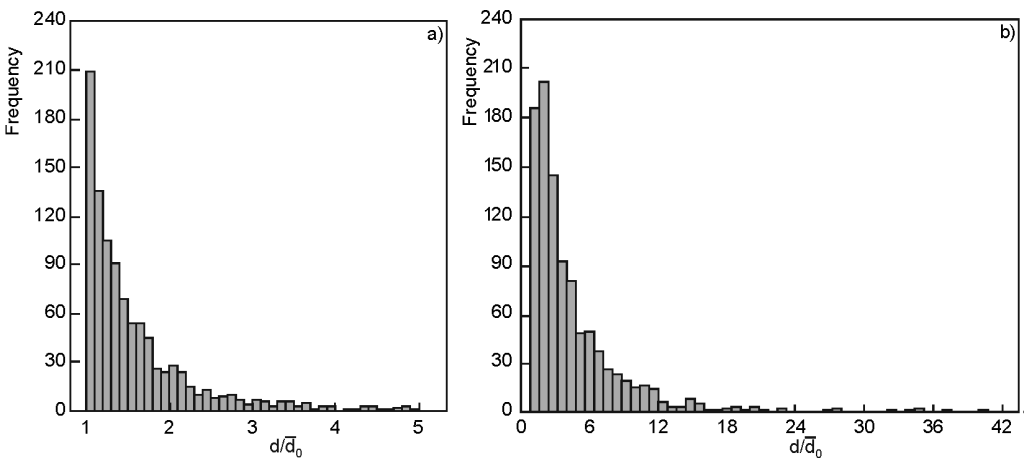

Fig. 2. Diameter distributions of the analyzed systems: a) power-law distribution with $a = -3.3$, b) log–normal distribution with parameters $\mu = 1.0$ and $\sigma = 0.9$

This optimization series was refined with a reduced range of standard deviation from 0.85 to 1.15 and smaller steps (step width 0.05). The above conjectured optimum value of $\sigma = 0.90$ could be verified here. The systems analyzed in the following were generated using this optimized log–normal pore size distribution and the optimized power-law pore size distribution given in [5].

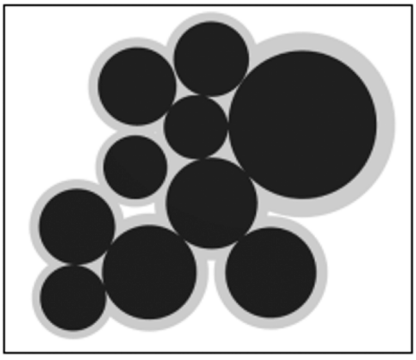

Fig. 3. Cherry-pit extension of a 2D disc system. The shells are increased proportional to their diameters. Dark discs are hard discs, the shell around is shown in gray. Shell diameters are calculated by $D_{shell} = (1+ m)D_{sphere}$ with $m = 0.25$

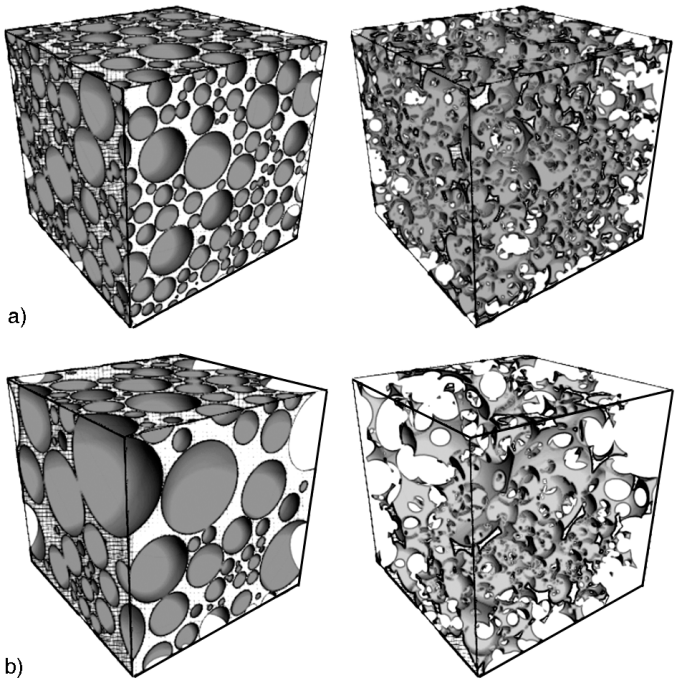

Fig. 4. Sectional view of model pore systems: a) power-law distributed diameters with $m = 0$ (closed pores, left) and $m = 0.15$ (open pores, right), b) log–normal distributed diameters, with $m = 0.0$ (closed pores, left) and $m = 0.15$ (open pores, right)

The generated porous systems are systems with closed pores due to the hard sphere properties of the sphere packing algorithm described in [7, 8]. To generate open

pore systems, we extended our packings to the cherry-pit model as described in [9]. This model is characterized by the fact that hard spheres feature a defined shell wherein they may overlap so they are partially penetrable. In Figure 3, a 2D representation of a sample model is shown to illustrate this principle.

There exist alternatives to create cherry-pit extensions of hard sphere systems. One approach is to increase all spheres with the same additive value, another one is to increase the diameters proportional to the hard sphere diameter. Because of the desired conservation of size distribution, we used here the latter one, the shell diameters are calculated according to equation $D_{\text{shell}} = (1+ m)D_{\text{sphere}}$.

The optimized log-normal and power-law distribution structure referred to in [5] were transformed to open pore structures according to the above mentioned cherry-pit model. The value of the scaling factor m was increased in 0.05 steps from 0 (closed pores) to 0.50. In Figure 4, one can see sectional views of sample systems. Figure 4a shows the power-law distributed porous model with closed pores (left) and increased pores (right, for m = 0.15), likewise Fig. 4b shows the log–normal distributed model with closed and open pores with the same parameter m.

4. Process simulation and properties

One of our intentions is to show that experimental results and simulated processes evidence a comparable behaviour. Positron annihilation lifetime spectroscopy is one of the experimental methods to characterize the porosity of materials [4]. The main principle is that the lifetime of a positronium – an atom-like couple of electron and positron – strongly depends on the free way of a particle. The larger the pores are, the longer the positronium lives – up to the maximum lifetime of 142 ns. When positroniums collide with a pore wall or when their lifetime is over, their components are annihilated to gamma radiation. This radiation and the time difference between formation and annihilation can be measured. The procedure is very appropriate for nanosized pores which cannot be normally investigated by traditional procedures like mercury porosimetry. In open pore systems, the average pore diameter can be estimated, in closed pore systems even the pore size distribution can be measured. In our simulations, the process of positronium implantation and lifetime measurement is calculated in a first approximation by random dimensionless particles which perform a non lattice-confined random walk through the simulated pore systems. In the following, this calculation process is described and some first results are given.

$$R(N) = \left|P_{\text{start}} - P_N\right| \tag{3}$$

$$t(N) = \frac{1}{V}\sum_{1}^{N}\left|P_{i+1} - P_i\right| \tag{4}$$

Particles without geometrical dimension are sequentially generated in the pores. A particle gets a random start vector and then it moves through the system. Reflections at the pore walls change the way of the particle according to the reflection laws. Positions P_{start}, P_i and P_N denote the starting point, intermediate points of reflection and the final position of the particle after N reflection events. After these reflections, the random walk of a particle ends at the position P_N. The effective covered distance $R(N)$ is calculated as the Euclidian distance between start position P_{start} and the particles final position after N reflections. The lifetime $t(N)$ is calculated as a quotient of the whole covered distance between all N reflections and assumed constant velocity V (Eqs. (3) and (4)). The porous model is assumed to be capped.

Another important property is the penetrability of open and closed pore systems. The penetrability for gases or fluids is one of the most important characteristics [3]. Interlayer dielectrics should not only avoid leakage current, they also protect the conducting layers. This protection is endangered when fluids or gases interfuse the dielectrics. Like in the simulations described above, a number of dimensionless particles are generated and sent through the system. All particles are generated at coordinates $p_i < 0, y_i, z_i>$ of the simulation volume with randomly generated y and z coordinates. Every particle gets a random directional vector which points into the simulation volume. The porous material is represented by our sphere packings described above with optimized log–normal and power-law distributions. The degree of open porosity varies from $m = 0$ (completely closed pores) to $m = 0.30$ (this means that all pores are scaled to 130% of their original diameters). All porous models are assumed as capped. The analyzed parameter is the maximum depth all particles reached. Mean depth and the maximum depth can show critical characteristics of variably parameterized porous systems.

5. Results

Analyzing the time after N reflections and the effective covered distance of particles in several pore size distributions with variable open porosity, one can see that for closed pores the estimated lifetime corresponds directly to the pore size distribution. There is a qualitative important leap in the behaviour from closed pores to pores with 5% overlap. Figure 5 shows that the more open the pore structure is, the better the estimated distribution of lifetimes approximate Gaussian behaviour. Mean lifetime increases because of the longer collision-free path of the particles. The distance covered and the lifetime of particles trivially increase heavily with increasing overlap of pores.

The flow rate $F(N)$ is defined as the ratio of the number of flown-through particles after N reflections $n_{\text{flow}}(N)$ and the number of all particles n_{all} (Eq. (5)). The flow rate was analyzed for 10 000 particles which are generated at coordinates $p_i < 0, y_i, z_i>$. A particle is declared as flown through when it reaches the opposite side of the simula-

tion box. This rate is zero in closed pore systems except for systems where the layer thickness is smaller than the maximum pore diameter. Simulations showed a critical point where the flow rate is rapidly increasing. At this point, the system becomes "transparent" for moving particles. These points differ for diverse pore size distributions and overlaps of pores

$$F(N) = \frac{n_{flow}(N)}{n_{all}} \tag{5}$$

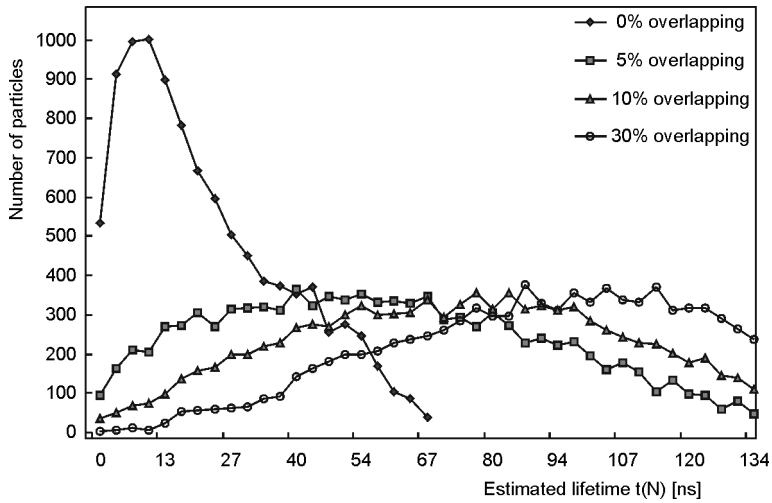

Fig. 5. Distribution of the estimated lifetime $t(N)$ for 10 000 particles and number of reflections $N = 50$ in a log–normal distributed pore system with various degrees of open porosity

The flow rate of particles passing through the system increases with increasing diameters (Fig. 6a). The diffusion resistance of the power-law structure is higher than the resistance of the log-normal system in case of equal porosity. The point where particles begin to flow through the system is increasing with $m = 0.15$ for the power-law system whereas this point is just reached below $m = 0.05$ for the log-normal system. For the power-law system one can say that this critical point is more definitely marked as for the log-normal system.

Mean interpenetration depth of particles in closed pore systems show stability against exogenous influences like vapor. Like in the simulations before, randomly generated particles are sent on one side to the surface of the pore system. They survive a predefined number of reflections with the pore walls. The deepest point reached by one particle is saved. In Fig. 6b one can see that this increases with increasing overlap of pores and differs for various pore size distributions. The distribution of the particle penetration depth is according to the depth profile of the surface in case of closed pores. With increasing open porosity the mean and maximum penetration depths increased.

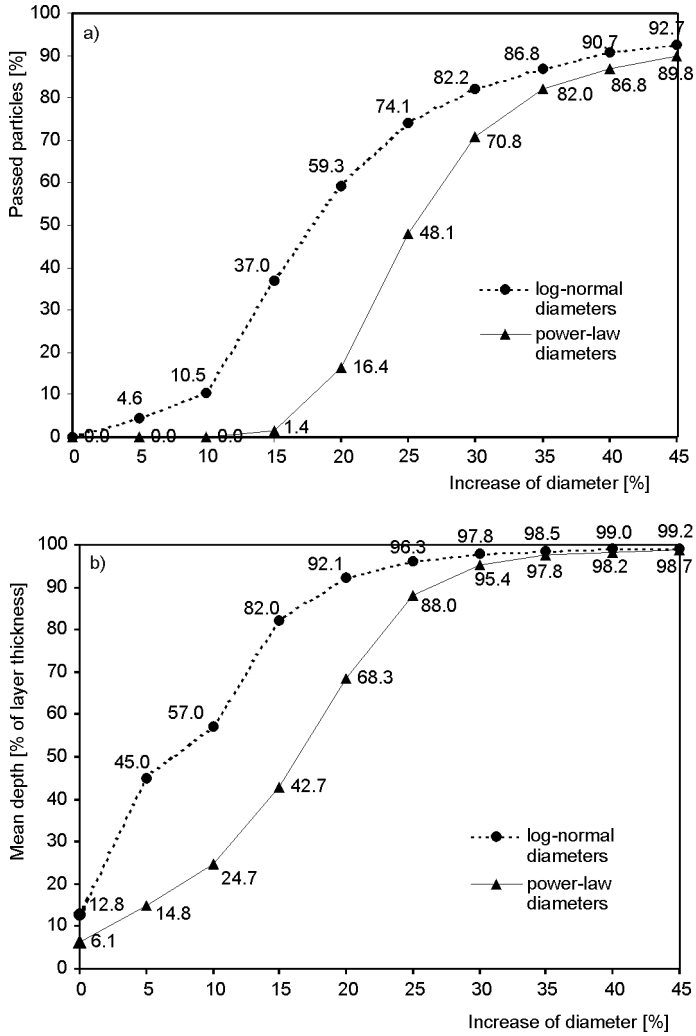

Fig. 6. Flow rates and mean penetration depths for capped porous layers with the thickness of 20 a.u. and $N = 50$ reflections: a) flow rate for 10 000 particles in a log-normal and a power-law porous system with different degree of open porosity, b) mean penetration depth of 10.000 particles for the same systems like above

A number of random walk particles is generated in the center of the simulation box under non-periodic boundary conditions. The system boundary is capped so that no particle can escape from the system. The mean squared distance R^2 is calculated and compared against passed time for assumed constant velocity (see Fig. 7).

The theoretical diffusion coefficient for dimensionless particles was estimated from these data for systems with both power-law and log-normal size distribution.

$$D = \frac{\overline{R^2}(N)}{6\,t(N)} \tag{6}$$

It was calculated according to the above given Eq. (6).

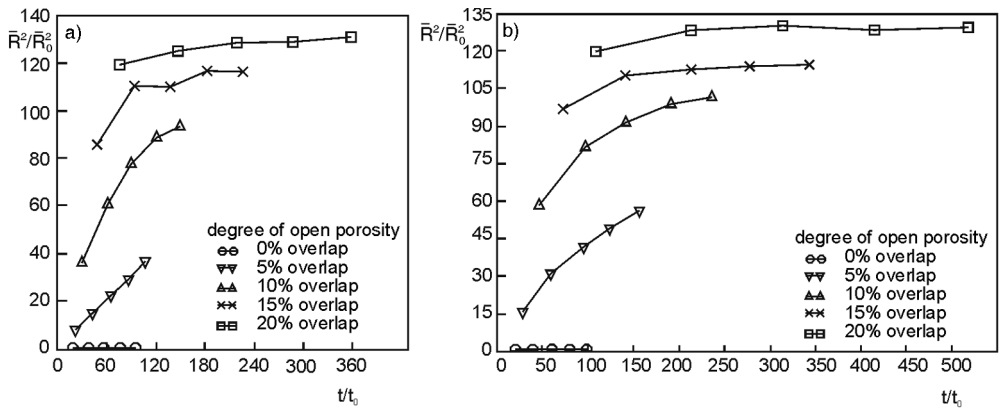

Fig. 7. The mean squared distance of particles to their start point against elapsed time calculated for constant velocity and different degrees of diameter increasing: a) for power-law distributed pores with $N = 50$ reflections, b) for log-normal distributed pores with $N = 50$ reflections

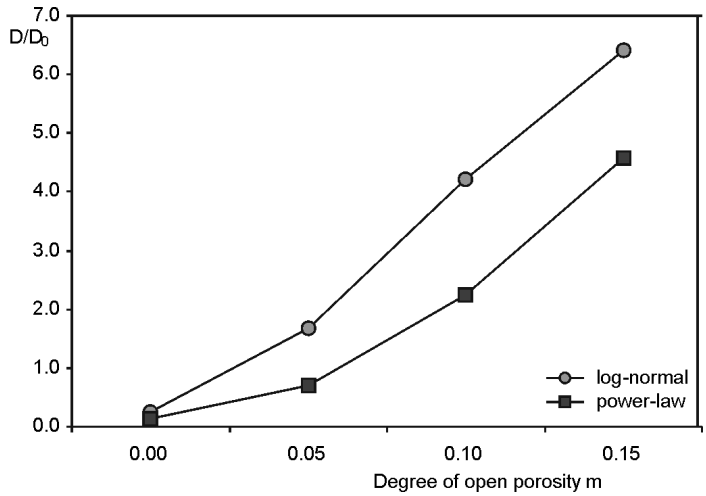

Fig. 8. Estimated diffusion coefficient for closed pores and open pores from $m = 0.05$ to $m = 0.15$

The power-law system shows a lower increase of the diffusion constant with increasing scaling factor m as the log-normal system. The general behaviour of the diffusion coefficients is similar in both pore size distributions and agrees with results given in [3].

6. Conclusion

Computer simulations of porous systems based on dense packed spheres are an appropriate model for the estimation and calculation of properties of real porous media. Low-*k* dielectrics of the porous type require a detailed control of their properties, because some desired properties are negatively correlated. Simulations as described are a useful method to optimize these properties and investigate the influence of one parameter on the others. The model of dense packed hard spheres was extended to the cherry-pit model to simulate open porous systems. Properties resulting from open porosity are estimated. The preferred pore size distribution is the power-law distribution with an exponent of $a = -3.3$ whereas the log–normal distribution showed an unfavourable behaviour.

Simulated flow rates of particles in finite porous systems show that diffusion behaviour for log–normal porous models seems to be less favourable than for the power -law models. The flow rate trivially increases with the increasing diameter scaling factor m. All analyzed model systems suggest that not only the value of porosity but also the pore diameter distribution and the degree of pore overlapping influence the properties of porous dielectric media. Additional simulations with described model systems should show further important properties of porous dielectrics like mechanical strength and thermal conductivity.

Acknowledgements

This work was supported by the Deutsche Forschungsgemeinschaft.

References

[1] GLADKOV S. O., *Dielectric Properties of Porous Materials*, Springer, Berlin, 2003.
[2] PLAWSKY J.L., GILL W.N., JAIN A., ROGOJEVIC S., *Nanoporous dielectric films: fundamental property relations and microelectronics applications*, [in:] *Interlayer Dielectrics*, S.P. Murarka, M. Eizenberg, A.K. Sinha (Eds.), Elsevier, Amsterdam, 2003, pp. 261–325.
[3] SHAMIRYAN D., BAKLANOV M.R., LYONS P., BECKX S., BOULLART W., MAEX K., Coll. Surf. A: Physicochem. Eng. Aspects, 300 (2007), 111.
[4] PENG H.-G., VALLERY R.S., LIU M., SKALSEY M., GIDLEY D.W., Col. Surf. A: Physicochem. Eng. Aspects, 300 (2007), 154.
[5] HERMANN H., ELSNER A., HECKER M. AND STOYAN D., Microel. Eng., 81 (2005), 535.
[6] NELDER J.A., MEAD R., Comput. J., 7 (1965), 308.
[7] JODREY W.S., TORY E.M., Phys. Rev. A, 34 (1986), 675.
[8] BEZRUKOV A., BARGIEL M., STOYAN D., Part. Part. Syst. Charact., 19 (2002), 111.
[9] A. R. KANSAL, S. TORQUATO, F. H. STILLINGER, J. Chem. Phys., 117 (2002), 8212.

Received 15 June 2007
Revised 19 November 2007